Report Documentation Page

Public reporting burden for the collection of information is estimated to average 1 hour per response, including the time for reviewing instructions, searching existing data sources, gathering and maintaining the data needed, and completing and reviewing the collection of information. Send comments regarding this burden estimate or any other aspect of this collection of information, including suggestions for reducing this burden, to Washington Headquarters Services, Directorate for Information Operations and Reports, 1215 Jefferson Davis Highway, Suite 1204, Arlington VA 22202-4302. Respondents should be aware that notwithstanding any other provision of law, no person shall be subject to a penalty for failing to comply with a collection of information if it does not display a currently valid OMB control number.

1. REPORT DATE **01 APR 2008**	2. REPORT TYPE	3. DATES COVERED

4. TITLE AND SUBTITLE **A First-Order Model of Thermal Lensing in a Virtual Eye**	5a. CONTRACT NUMBER **F4162402-D-7003**
	5b. GRANT NUMBER
	5c. PROGRAM ELEMENT NUMBER **61102F**

6. AUTHOR(S) **Rebecca Vincelette; Robert Thomas; Benjamin Rockwell; Clifton Clark**	5d. PROJECT NUMBER **2312**
	5e. TASK NUMBER **AH**
	5f. WORK UNIT NUMBER **02**

7. PERFORMING ORGANIZATION NAME(S) AND ADDRESS(ES) **Air Force Research Laboratory, 711 Human Performance Wing ,Human Effectiveness Directorate, Directed Energy Bioeffects Division,Optical Radiation Branch and University of Texas at San Antonio ,Brooks City-Base,TX,78235-5214**	8. PERFORMING ORGANIZATION REPORT NUMBER **UTSA, 711 HPW/RHDO**

9. SPONSORING/MONITORING AGENCY NAME(S) AND ADDRESS(ES)	10. SPONSOR/MONITOR'S ACRONYM(S)
	11. SPONSOR/MONITOR'S REPORT NUMBER(S)

12. DISTRIBUTION/AVAILABILITY STATEMENT
Approved for public release; distribution unlimited.

13. SUPPLEMENTARY NOTES

14. ABSTRACT

15. SUBJECT TERMS

16. SECURITY CLASSIFICATION OF:			17. LIMITATION OF ABSTRACT	18. NUMBER OF PAGES **11**	19a. NAME OF RESPONSIBLE PERSON
a. REPORT **unclassified**	b. ABSTRACT **unclassified**	c. THIS PAGE **unclassified**			

First-order model of thermal lensing in a virtual eye

Rebecca L. Vincelette,[1,]* Robert J. Thomas,[2] Benjamin A. Rockwell,[2] Clifton D. Clark III,[3] and Ashley J. Welch[1]

[1]*University of Texas at Austin, Department of Biomedical Engineering, Cockrell School of Engineering,*
1 University Station C0800, Austin, Texas 78712, USA
[2]*Air Force Research Laboratory, 2624 Louis Bauer Dr., Brooks City-Base, Texas 78235, USA*
[3]*Northrop Grumman, 2624 Louis Bauer Dr., Brooks City-Base, Texas 78235, USA*
*Corresponding author: rebecca.vincelette@gmail.com

An *ABCD* beam-propagation method was used to build a first-order mathematical model of a thermal lens effect from a near-infrared laser beam in water and ocular media. The model was found to fit experimental z-scan data best when the thermo-optic coefficient dn/dT of liquid water at 292 K was -4.46×10^{-5} K^{-1}. The physiological parameters of the human eye were simulated in a simple eye model using this fitted dn/dT value. Conservative model simulations for 1150 and 1318 nm laser radiation include parameter sets used in experimental ocular exposures performed by Zuclich *et al.* [Health Phys. **92**, 15 (2007)] to illustrate the transient response of the thermal lens approaching the limits of the retinal damage thresholds for equivalent laser radiation sources. © 2009 Optical Society of America

OCIS codes: 330.3350, 190.4710, 120.6810, 170.1020, 170.3660.

1. INTRODUCTION

Laser safety for the retina is established by experimental studies at many wavelengths and exposure durations to determine the smallest pulse energy into the eye that produces a minimum visible lesion (MVL) as seen with a fundus camera. Retinal MVLs determined in the near-infrared (NIR) region are higher than expected and suggest some unexplained laser–tissue interactions [1]. We believe thermal lensing plays a significant role in laser–tissue interactions influencing ocular damage for wavelengths from 1150–1350 nm, where preretinal media strongly absorb laser radiation, yet there is enough energy remaining to pose a threat to the sensitive retinal layers.

Thermal retinal damage models use laser-induced heat generation, heat conduction, and the Arrhenius damage integral to predict the formation of a laser-induced lesion in the retina [2]. These models require an understanding of laser beam spot size and energy at the retina that depend on optical properties of the preretinal media including dispersion, absorption, and physical dimensions of the eye. Similar fundamental understandings are necessary to estimate an action spectra used to make predictions on general trends by fitting available MVL data over the entire UV–visible–IR spectrum [1,3–5]. To date, thermal lensing has been a relatively unexplored laser–tissue interaction in the eye and has not been incorporated in any eye model used to predict retinal damage thresholds.

The discovery of thermal lensing by Gordon *et al.* in 1965 led to the development of numerous mathematical models [6]. The phenomenon is the result of a temperature gradient, typically assumed to be radially symmetric, formed by the absorption of laser light in the medium. As the temperature T of the medium increases, the local density ρ decreases. This leads to a decrease in the index of refraction n resulting in the formation of a negative lens. The temperature gradient is shaped by the beam profile and the thermal diffusivity of the medium [7–10]. The creation of a thermal lens in ocular media means the spot size formed at the retina changes dynamically as a function of the coupled transient response of heat generated by the beam profile and thermal diffusion.

Many thermal lensing models begin with a solution of the heat conduction equation in combination with an *ABCD* ray-tracing method [9–11]. The model assumes a radially symmetric temperature gradient in an absorbing medium where no heat is exchanged along the optical axis z.

A closed-aperture z-scan is one technique to correlate transmission data through an absorbing medium to a thermal lens gradient [12]. A single-beam, closed-aperture z-scan using 1313 nm light provides an estimate of thermal lensing in water. The thermal characteristics of water are well documented and show similar linear absorption coefficients to those of ocular media at NIR wavelengths, making the z-scan a basic method for initial evaluation of the thermal lensing model [13–17].

In this paper, data from a single-beam, closed-aperture z-scan using a continuous wave (CW) 1313 nm laser radiation source are presented and compared with a first-order model for thermal lensing. Data from the z-scan are used to determine an estimate of the change in index of refraction with the change in temperature dn/dT for this region of laser radiation. Having demonstrated a reasonable fit to z-scan data, the first-order model is then used as a tool for predicting trends of the thermal lensing effect in a virtual eye. Preliminary data relating to this work have been reported [18–21]. The first-order model pre-

sented here does not include heat conduction along the
z-axis nor the effects of convection in the absorbing me-
dia. The more viscous properties of ocular media com-
pared with water preclude significant convectional flow.

2. BACKGROUND

A. Z-Scan Spectroscopy
The z-scan is a common analytical technique used to mea-
sure the thermal lens effect. The technique is a well es-
tablished method in chemistry for chromatography and
electrophoresis analyses and in electro-optics for testing
the characteristics of optical limiters [7–12].

A single-beam z-scan is the simplest of z-scan tech-
niques, where a single laser is used as the pump and
probe. The laser beam is collimated and aligned to be sent
through a focusing lens. A chopper or shutter placed after
the focusing lens is traditionally used as the control for
the exposure duration [12]. The sample is placed at posi-
tion z in the beam's path after the shutter and at an angle
just a few degrees from the z axis to prevent reflective in-
terference from the cuvette windows. A detector is placed
in the far field from the focusing lens. An aperture is
placed just in front of the detector, giving the nomencla-
ture of a "closed-aperture z-scan." Irradiance data are col-
lected as a function of time as the sample is held in a sta-
tionary position. The sample is allowed time to relax back
to its initial thermal state, then moved to a new z position
before beginning the next exposure. Conventional z-scan
data report the z-position of the sample in relation to the
distance from the focal plane of the focusing lens. The ab-
sorption of laser radiation in liquid media causes the for-
mation of a negative thermal lens. The irradiance mea-
surements are analyzed at a selected time and
normalized to a reference irradiance signal taken for the
sample placed at a far distance—approximately one focal
length—from the focus of the lens (Fig. 1). The z-scan
data [Fig. 1(d)] depict an increase [Fig. 1(b)] and decrease
[Fig. 1(c)] in relative irradiance for sample positions be-
fore and after the focus, respectively, with an inflection
point occurring at the focal plane of the lens [Fig. 1(a)].

Selections of the lens and the sample thickness are im-
portant for the z-scan. The irradiance of the thermal lens
is largely related to the generation of heat [W/m³] in the
sample, making the choice of a short focal length lens
seem desirable. However, since the thermal lens measure-
ment is very sensitive to confocal distance, Franko and
Tran describe using a sample thickness T_S that is at least
one-third or less than the confocal distance:

$$T_S \leq \frac{1}{3}\frac{2\pi\omega_{min}^2}{\lambda}, \tag{1}$$

where ω_{min} is the minimum $1/e^2$ beam waist radius of the
probe beam with wavelength λ [12]. The minimum waist
can be approximated as $f\lambda/2d$ where d is the beam's $1/e^2$
diameter at the focusing lens with focal length f. As a re-
sult, the selected sample path length is proportional to
the confocal distance, or twice the Rayleigh range, of the
system design.

A single-beam, closed-aperture z-scan allows for the
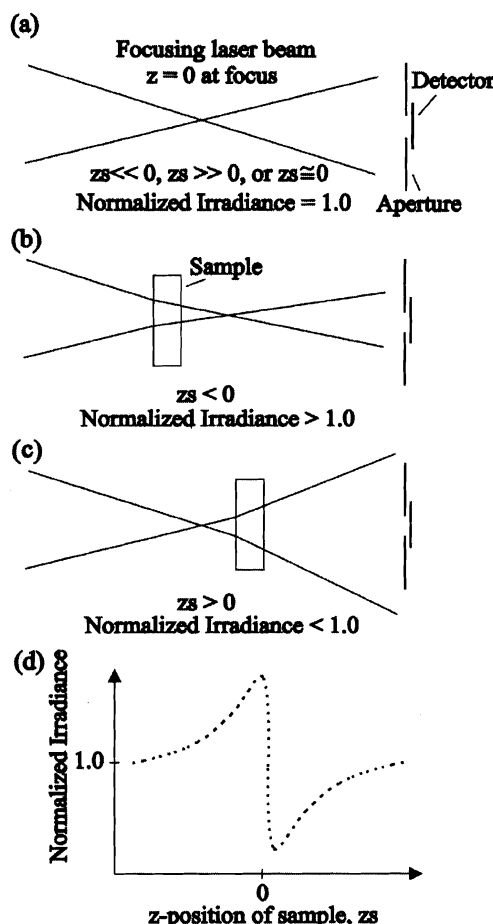transient information of only the excitation of the sample

Fig. 1. Example of a negative thermal lens z-scan. The cases for
the samples exposed at the z positions: (a) very far from the focus
of the lens and very near or at the focus resulting in unity nor-
malized irradiance, (b) before the focus resulting in an increase
in normalized signal irradiance, and (c) after the focus resulting
in a decrease in signal irradiance. (d) Resulting z-scan data set.

[12]. When both the excitation and relaxation of the
sample are desired, a dual-beam z-scan should be used.

B. Mathematical Model
Using Yariv's approach for deriving the relationship of a
medium with a quadratic index of refraction to a ray, the
index of refraction n can be described as a function of ra-
dial distance r from the optical axis z and temperature T
[11]. Using a Maclaurin series to expand an expression for
$n(r,T)$ gives

$$n(r,T) = n_o + r\left(\frac{\partial n}{\partial r}\right)_{r=0} + \frac{r^2}{2!}\left(\frac{\partial^2 n}{\partial r^2}\right)_{r=0} \ldots. \tag{2}$$

Truncating the series and applying the chain rule gives

$$n(r,T) = n_0 + r\left(\frac{\partial n}{\partial T}\frac{\partial T}{\partial r}\right)_{r=0} + \frac{r^2}{2}\frac{\partial}{\partial r}\left(\frac{\partial n}{\partial T}\frac{\partial T}{\partial r}\right)_{r=0}. \tag{3}$$

The change in temperature with respect to radial distance
at radial position $r=0$ can be set to zero, simplifying the
expression to just the background index of refraction n_0

and the last term containing the square of the radius r. From this point, applying the product rule gives an expression that is then evaluated for $\partial T/\partial r \rightarrow 0$ at $r=0$, where the maximum irradiance of the beam is found, revealing the expression

$$n(r,T) = n_0 + \frac{r^2}{2}\left[\frac{\partial}{\partial r}\left(\frac{\partial n}{\partial T}\right)\right]\frac{\partial T}{\partial r}^{r=0} + \frac{r^2}{2}\left[\frac{\partial}{\partial r}\left(\frac{\partial T}{\partial r}\right)\right]\frac{\partial n}{\partial T}^{r=0},$$

(4)

which further reduces to

$$n(r,T) = n_0 + \frac{r^2}{2}\frac{\partial^2 T}{\partial r^2}\frac{\partial n}{\partial T}^{r=0}.$$

(5)

The background index of refraction n_0 must be selected for the corresponding medium and wavelength of interest. The term $\partial^2 T/\partial r^2$ is solved using a Green's function solution to the heat conduction equation, explained below [8–10]. For cases where the laser pulse is longer than the acoustic transit time, as is the case with CW laser exposures, the change in n, Δn, can be approximated by $(dn/dT)(\Delta T)$ [7]. The term dn/dT is referred to as the thermo-optic coefficient and is wavelength dependent [8,22].

An equivalent expression for $n(r,T)$ for a medium with a quadratic index of refraction is described by Yariv as [11]

$$n = n_0\left(1 - \frac{Xr^2}{2}\right).$$

(6)

A solution for X is determined by considering only CW cases and setting Yariv's equation for n, Eq. (6), equal to the solution for $n(r,T)$, Eq. (5), giving

$$X = \frac{1}{n_0}\frac{dn}{dT}\frac{\partial^2 T}{\partial r^2}.$$

(7)

The term X is needed to describe how a ray would move through a quadratic-index medium using an *ABCD* propagation matrix. The *ABCD* matrix for propagating a beam through a negative-lenslike medium is given as [11]

$$\begin{bmatrix} A & B \\ C & D \end{bmatrix} = \begin{bmatrix} \cosh(X^{1/2}\Delta z) & X^{1/2}\sinh(X^{1/2}\Delta z) \\ X^{1/2}\sinh(X^{1/2}\Delta z) & \cosh(X^{1/2}\Delta z) \end{bmatrix}$$

(8)

The term Δz is the axial step or length of the step through which the beam is propagating. A complex beam parameter $q(z)$ is used to describe the ray at position z anywhere along the z axis in a medium as

$$q(z)_{new} = \frac{Aq(z)_{old} + B}{Cq(z)_{old} + D}.$$

(9)

The complex beam parameter is described by the real and imaginary portions of a wavefront by

$$\frac{1}{q(z)} = \frac{1}{R(z)} - i\frac{m^2\lambda}{\pi\omega(z)^2},$$

(10)

where the real portion of the complex beam parameter contains information about the radius of curvature $R(z)$, while the imaginary portion contains the wavelength tra-

versing the medium and the $1/e^2$ beam radius $\omega(z)$. The value of m^2, or m-squared, describes the quality of collimation of the beam [23,24]. Ideally, a Gaussian beam would have an m^2 value of 1.0, but realistically, the value is greater than 1.0.

To solve for the $\partial^2 T/\partial r^2$, the eye can be treated as a cylindrically symmetric medium with thickness z. For our first-order model, thermal diffusion along the optical axis is assumed to be zero ($\partial T/\partial z=0$). Thus, we assume diffusion occurs along the radial direction. However, the heat-source term $S(z)$ is attenuated in the z direction according to Beer's Law [see Eq. (15) below]. The thermal diffusion equation,

$$\frac{1}{r}\frac{\partial}{\partial r}\left[\kappa r\frac{\partial T}{\partial r}\right] + S(z) = \rho c_p\frac{\partial T}{\partial t},$$

(11)

must be solved first by differentiating the heat equation with respect to $T(\mathbf{r},t)$, then integrating to find $\partial^2 T/\partial r^2$. Here t is time, r is the magnitude of the radial vector described by position (x,y), η is the thermal diffusivity in cm^2/s, and $S(z)$ is the source term. Note: $\eta = \kappa/\rho c_p$ where κ is the thermal conductivity in W/cm K, ρ is the density in g/cm^3, and c_p is the specific heat at constant pressure in J/g K.

We modeled our eye as an infinite cylinder with heat generation originating from the Gaussian beam launched into the eye. Since the conduction of heat is assumed to be purely a radial process, the diffusion equation is independent of angle and axial position, allowing the radial vector $\mathbf{r}$ to reduce to a scalar radial magnitude r [25,26]. Applying the product rule and rearranging variables in Eq. (11) gives the heat equation

$$\frac{\partial^2 T}{\partial r^2} + \frac{1}{r}\frac{\partial T}{\partial r} + \frac{1}{\kappa}S(z) = \frac{1}{\eta}\frac{\partial T}{\partial t}.$$

(12)

The Green's function for a virtual cylindrical eye with no diffusion along z is taken as

$$G(r,t;r',t') = -\frac{1}{4\pi\eta(t-t')}$$
$$\times \exp\left[-\frac{(r^2+r'^2)}{4\eta(t-t')}\right]I_0\left[\frac{rr'}{2\eta(t-t')}\right],$$

(13)

where r' describes the position of the cylindrical surface heat source, and I_0 is the modified Bessel function of the first kind [10,26]. The units of this Green's function are in cm^{-2}. $G(r,t;r',t')=0$ for all positions where r is on the surface of the cylindrical medium. Since only CW cases are being considered here, $t'=0$. Applying the Green's function Eq. (13) to the heat diffusion Eq. (12), for a symmetrical Gaussian beam results in

$$T(z,r,t) = \frac{1}{\rho c_p}\int_0^t dt'\int_0^{2\pi}d\theta\int_0^\infty r'dr'S(z,r')G(r,t;r').$$

(14)

The expression

$$S(z,r') = \frac{2\mu_a P_z}{\pi\omega^2} \exp\left[\frac{-2(r')^2}{\omega^2}\right] \qquad (15)$$

describes the source term $S(z,r')$ for the symmetrical Gaussian beam; for the eye in W/cm^3 it can be found by applying Beer's law assuming a Gaussian beam [9,10]. In Eq. (15), μ_a is the linear absorption coefficient in cm^{-1}, ω is the $1/e^2$ beam radius, and r' denotes the location of the heat source. P_z is the power in watts delivered at position z in the sample, given by Beer's law as $P_z = P_0 \exp(-\mu_a z)$, with P_0 as the initial power delivered at the front surface of the sample. The power is expressed in an array of values by Beer's law through $P_{z+\Delta z} = P_0 \exp(-\mu_a z)\exp(-\mu_a \Delta z)$, where z is the position along the z axis within the sample and Δz is the same spatial step described earlier in Eq. (8).

Using Mathematica 5.2, a solution for $\partial^2 T/\partial r^2$ was verified to be

$$\frac{\partial^2 T}{\partial r^2} = \frac{-\eta 8 \mu_a P_z}{\pi\kappa\omega^2}\left[\frac{t}{8\eta t + \omega^2}\right]. \qquad (16)$$

The beam and subsequent radial temperature profiles are assumed to be Gaussian over all time t. The critical time is defined by $t_c = \omega^2/8\eta$, allowing the solution to reduce to

$$\frac{\partial^2 T}{\partial r^2} = \frac{-\mu_a P_z}{\pi\omega^2\kappa}\left[\frac{1}{1 + t_c/t}\right]. \qquad (17)$$

Analysis of the problem can include observing the temperature rise along the optical axis. Given our assumption of $\partial T/\partial z = 0$ and initial condition $\partial T/\partial t = 0$, the temperature rise along the z axis is representative of the central temperature resulting from diffusion along the radius r. The temperature rise along the z axis at $r=0$ is then determined by evaluating the heat conduction equation at $r=0$, giving [this requires applying L'Hôpital's Rule to the term $(1/r)\mathrm{d}T/\mathrm{d}r$]

$$\left(\frac{\partial T}{\partial t}\right)\bigg|_{r=0} = \eta\left(2\frac{\partial^2 T}{\partial r^2} + \frac{1}{\kappa}S(z)\right)\bigg|_{r=0}. \qquad (18)$$

The source term at $r=0$ simplifies to $S(z) = 2\mu_a P_z/\pi\omega^2$, where P_z was previously described. Numerical integration of Eq. (18) with respect to time can then be used to determine an approximate solution to the temperature T. We assume a uniform temperature T_0 when $t_0 = 0$ with an initial beam radius ω_0 created from the optical geometry of the system with no thermal lensing. Methods for solving this integral have been reported in Swofford and Morrell [27].

3. MATERIALS AND METHODS

A. Single-Beam, Closed-Aperture Z-Scan
A 1313 nm IRCL-150-1313-P-L CrystaLaser was collimated and aligned (Fig. 2) to create a $1/e^2$ beam diameter at the focusing lens of 3.5 mm and an m-squared of 1.16. A 400 mm BK7 planoconvex lens was used as the focusing lens. A knife-edge test found the 1313 nm laser focus to be 42 cm from the center of the lens.

The power of the 1313 nm laser was attenuated by using a Thorlab NEK01 neutral density (ND) filter set. A
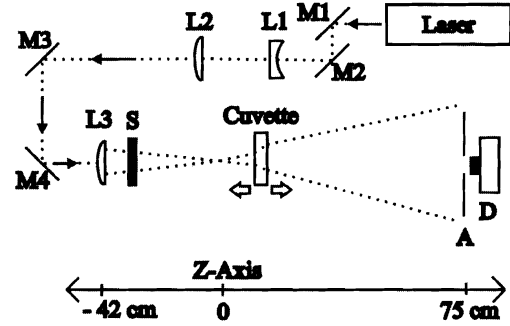

Fig. 2. Closed-aperture, single-beam z-scan set up. The z axis is referenced to the focal position of the lens found using a knife-edge technique in air, with no cuvette in the beam path. The laser was a 1313 nm CrystaLaser IRCL-150-1313-P-L. M1–M4, IR-coated mirrors; L1 and L2, IR-coated lenses created a beam expander of $\approx 1.5\times$; L3, 400 mm ThorLabs planoconvex 1 in. lens; SW, 1 cm diameter Uniblitz shutter; Quartz cuvette from Starna Cells; A, Aperture set to 2.5 mm diameter; D, 818-IR Newport detector.

Uniblitz 10 mm shutter was used to control the delivery of the laser beam to the sample. The focusing lens and any ND filters were placed before the Uniblitz shutter to allow for any thermal lens in the optical components to remain in steady state throughout the duration of the experiment.

All experiments were run at room temperatures between 17–20 °C. A sample of ultrapure deionized water was placed in a 10 mm quartz cuvette purchased from Starna Cells Inc. Samples were run in sets at 100 and 1000 ms exposures for powers of 2.60 and 48 mW. The linear absorption coefficient of water for 1313 nm was estimated to be 1.27 cm^{-1} [13].

A Newport 818-IR detector was placed 117 cm down the optical path from the focusing lens. A 2.5 mm aperture placed in front of the detector was found to yield the largest dynamic range in normalized irradiance data for our z-scan system. A detailed analysis of the selection of an aperture has been reported by Sheik-Bahae *et al.* [28]. The irradiance signal from the detector was sent to a Melles Griot large gain transimpedance amplifier before being recorded in Labview. A Stanford Research Systems signal delay generator was used to synchronize the data acquisition with the shutter. The sample was then placed on a stage along the optical path of the focusing lens ranging from -18 to 22 cm in 1 cm increments relative to the focal position of the lens. The irradiance values were normalized by values measured for a sample position at least 22 cm from the focus.

In earlier reports of our first-order thermal lensing model, we used constant thermal coefficients and discovered a strong sensitivity in our early model to small changes in these coefficients [18]. To model the z-scan experiments presented here, values for thermal conductivity κ, specific heat at constant pressure c_p, and density ρ as a function of temperature T were obtained from Wagner and Kruse at 0.1 MPa [15]. Data between 10–90 °C were fitted to a polynomial in EXCEL to obtain continuous temperature-dependent thermal properties. These polynomials are given in Table 1. Thermal diffusivity η was calculated from $\eta = \kappa/\rho c_p$, then fitted to a polynomial. The

Table 1. Thermal Couductivity κ, Density ρ, Specific Heat at Constant Pressure c_p, and Thermal Diffusivity η, As a Function of Temperature T Found to Fit Data for Liquid Water[a]for 0.1 MPa between 283.15 and 363.15 K

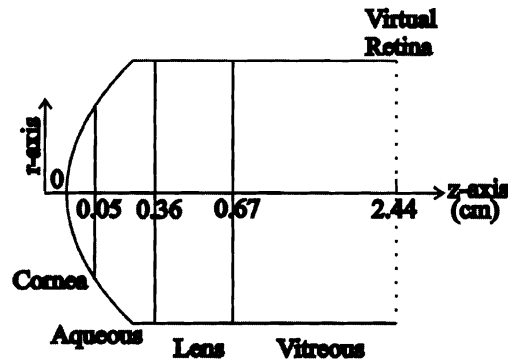| Symbol [Units]	Coefficient As a Function of Temperature, T [K]
κ [W/(cm K)] =	$-9.99 \times 10^{-3}T^2 + 7.649 \times 10^{-5}T \ldots$ -7.851×10^{-3}
ρ [g/cm^3] =	$-3.461 \times 10^{-6}T^2 + 1.798 \times 10^{-3}T \ldots$ $+7.684 \times 10^{-1}$
c_p [J/(g K)] =	$1.743 \times 10^{-9}T^4 - 2.322 \times 10^{-6}10^3 \ldots$ $+1.169 \times 10^{-3}T^2 - 2.632 \times 10^{-1}T \ldots$ $+2.649 \times 10^{1}$
η [cm^2/s] =	$-2.207 \times 10^{-3}T^2 + 1.778 \times 10^{-5}T \ldots$ -1.882×10^{-3}

[a]From Wagner and Kruse [15].

Fig. 3. Simple eye model with a radius of curvature of 0.61 cm on the front surface of the cornea brings a collimated 589 nm beam to a minimum at the virtual retinal plane 2.44 cm after the front surface of the eye. The vitreous layer is infinitely long, with beam trend observations made at the position of the virtual retina.

linear regression R^2 value was greater than 0.995 for all polynomial fits to the Wagner/Kruse data.

B. Model of the Virtual Eye

The eye is a complex optical system, but for our purposes in assessing trends of thermal lensing in an eye, we have simplified our model eye down to a basic compartmental system consisting of a single curved surface. Limitations regarding the simple eye model are reserved for the discussion. Thermal lensing in a simple eye model was simulated for two wavelengths: 1318 nm, as this was the wavelength used in retinal ED$_{50}$ studies by Zuclich *et al.* [3], and 1150 nm, to contrast variations in thermal lensing from a change in absorption coefficients. The eye was modeled as a four-chamber compartment partitioned into cornea, aqueous, lens, and vitreous chambers with a radius of curvature existing only on the front surface of the air–cornea boundary. This radius of curvature is essential in the *ABCD* beam propagation for our thermal lensing model. Linear absorption coefficients for each of these ocular media for 1150 and 1318 nm are in Table 2. A review of the literature found the average thickness of these chambers for a human to be 0.05, 0.31, 0.36, and 1.72 cm for cornea, aqueous, lens and vitreous, respectively (Fig. 3) [29–31]. With a known refraction and physiological distance to a virtual retinal plane of 2.44 cm, a radius of curvature r_c of 0.61 cm was found to set the 589 nm wavelength to a minimum focus at $z = 2.44$ cm.

Refractive error measurements for wavelengths beyond 900 nm in the eye are limited, thus chromatic dispersion for wavelengths greater than 900 nm were based on data trends in Fernández *et al.* [32]. Using these trends in refractive error, a bulk refractive index value as a function

of wavelength was determined by a Sellmeier fit, as described in an earlier publication by Vincelette *et al.*, to account for chromatic dispersion in our eye model [1]. For a given wavelength, the initial values of $\omega(z)$ in the virtual eye are calculated from the *ABCD* propagation method described by Yariv from Eqs. (6)–(10) using the corresponding bulk refractive index from the Sellmeier fit reported in Vincelette *et al.* [1]. The thermal conductivity κ specific heat at constant pressure c_p, and density ρ of ocular media were held as constants reported by Okuno *et al.* [33].

C. First-Order Thermal Lensing Mathematical Model

The mathematical model presented earlier was built in Matlab to predict the thermal lensing effect in a single-beam, closed-aperture z-scan and in the reduced eye model. The thermal lensing model requires an initial seed of $1/e^2$ beam-waist values based on no thermal lensing; these become the beam-waist values at $t = 0$ s. Subsequent $1/e^2$ waist values for $t > 0$ are then found through an iterative process using small time steps initially, gradually increasing the time step size as the thermal lens reaches steady-state.

A value for dn/dT was selected for the model based on a best fit to the z-scan data. This value of dn/dT was then used in modeling the thermal lensing effect in the simple eye model.

To determine the thermo-optic coefficient from literature, the index of refraction data at 0.1 MPa (~1 atm) for laser radiation at 404, 589, 632, 1013 and 2325 nm in water in the liquid phase between 10 and 90 °C as reported by Schiebener *et al.* were fitted to third-order polynomials in EXCEL to determine $n(T)_\lambda$ [16]. The first derivative was

Table 2. Linear Absorption Coefficients for Ocular Media and Water at 1150 and 1318 nm[a]

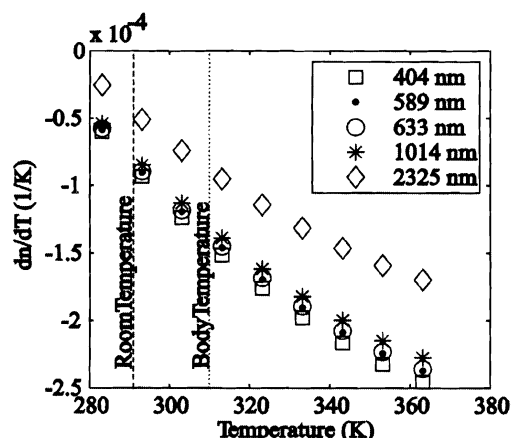| λ [nm]	Absorption Coefficient, μ_a [cm^{-1}]				
	Cornea	Aqueous	Lens	Vitreous	Water
1150	1.51	1.22	0.61	1.13	1.78
1318	1.98	2.01	0.97	1.90	1.34

[a]From [13,17].

Fig. 4.   Values of dn/dT (in K^{-1}) as a function of temperature for water in the liquid phase for five different wavelengths. Values here were based on taking the derivative of $n(T)_P$ at each of the five wavelengths as reported by Schiebener *et al.* at 0.1 MPa [16].

then taken from the fit to determine $dn/dT(T)$ for five different wavelengths as shown in Fig. 4.

4. RESULTS

A. Model Compared with Experimental Z-Scan Data
By substituting Eq. (17) into Eq. (7) and using the *ABCD* beam-propagation method described in Eqs. (8)–(10) the model was arranged to simulate the z-scan set up depicted in Fig. 2. A comparison of the results from this portion of the model to experimental z-scan data for varying input power and a 10 mm thick water-filled cuvette at room temperature can be found in Figs. 5 and 6. The z-scan data presented here reflect the average of three experimental runs. The standard deviation of the normalized intensity (for experimental data results) was approximately ±0.02 arbitrary units.

A bulk value of -4.46×10^{-5} K^{-1} for dn/dT was found to give the best fit to the experimental 1313 nm radiation z-scan data in terms of line width before and after the focal position at $z = 0$ and yielded the best approximation to

the slope between the maxima and minima. A detailed discussion of the impact of the value of dn/dT is reserved for later.

B. Thermal Lensing Model Trends in Virtual Eye
The dn/dT value found to fit the z-scan data was used in the simple eye model presented in Fig. 3 to make predictions on the trends of thermal lensing in a human eye. Analysis of the Schiebener *et al.* data [16] (Fig. 4) suggests that this value of dn/dT will approximately double when the ambient temperature is increased from room to body temperature. To test for the significance in this variation due to an increasing thermo-optic coefficient in our model, we used a constant dn/dT value of -4.46×10^{-5} K^{-1} for the results in Figs. 7–10 and then doubled dn/dT to -8.92×10^{-5} K^{-1} for the results in Fig. 11. Again, Eq. (17) was substituted into Eq. (7) and the *ABCD* beam-propagation method described in Eqs. (8)–(10) was used, except now the model was arranged to simulate the virtual eye (Fig. 3). All other values for the simple eye model have been previously described.

The influence of power from a Gaussian 1318 nm laser radiation source input into the eye on the beam's radius at the retina as a function of time is shown in Fig. 7. The results in Figs. 7 and 9–11 were normalized to the initial $t = 0$ beam radius at the retina in order to examine the magnitude of the increase in the beam's radius (i.e., a factor of two, ten, etc.) due to thermal lensing. Where appropriate, the value for normalizing the results is given in the caption. The 20 W case, shown in Fig. 7, represents the upper limit of the 1318 nm, CW laser radiation source that was used in CW nonhuman primate retinal damage studies conducted by Zuclich *et al.* [34].

Keeping the power delivered to the cornea at 3 W, the influence of the beam diameter from a Gaussian 1318 nm laser radiation source input at the cornea on the beam radius at the retina as a function of time is shown in Fig. 8. Parameters were for a 3 W, CW, 1318 nm laser radiation source delivering collimated $1/e^2$ Gaussian beam radii of 0.5, 0.75, 1.25, 1.75, and 2.25 mm at the virtual cornea. Note that Zuclich *et al.* reported the corneal ED_{50} for a CW, 1318 nm laser radiation delivered to the cornea for 0.28 s exposures is 0.56 J [34]. Zuclich *et al.* used a beam
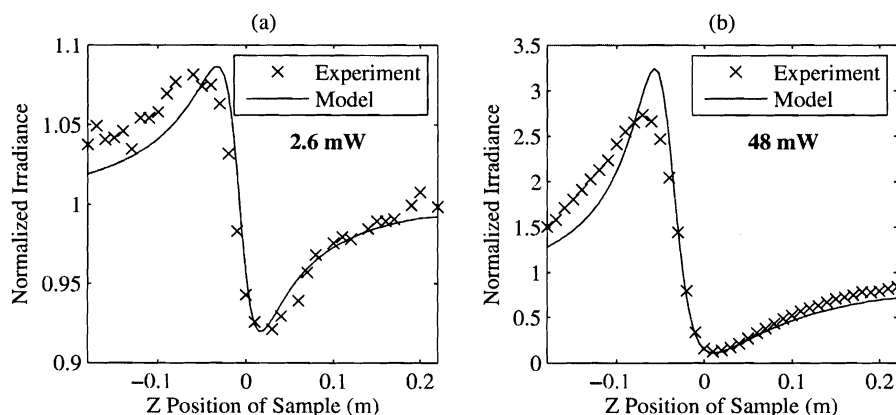

Fig. 5.   Z-scan data for a 10 mm water-filled cuvette exposed to 1313 nm CW laser source for 1 s at (a) 2.6 mW and (b) 48 mW. The time response for the maxima and minima from each peak can be found in Fig. 6.
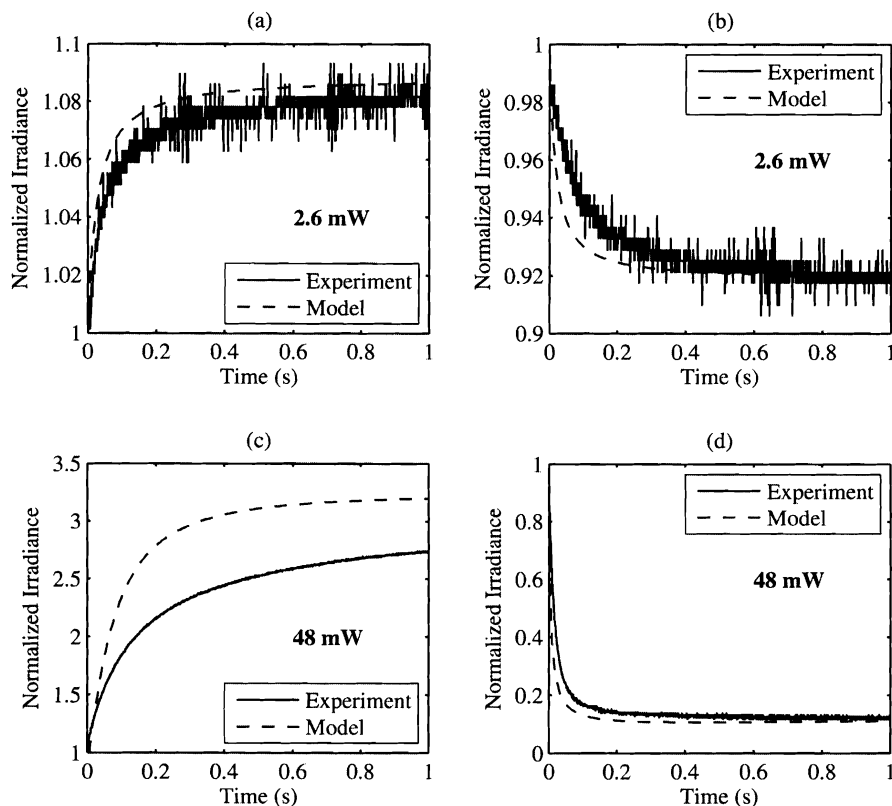
Fig. 6.   Transient response for the z scan peaks from Fig. 5 for 2.6 mW (a) maximum and (b) minimum and 48 mW (c) maximum and (d) minimum.

radius of 0.5 mm at the cornea, giving an ED_{50} of approximately 72 J/cm^2. The point in time at which each of the 0.5, 0.75, 1.25, 1.75, and 2.25 mm beam radii at the cornea begins to exceed the 72 J/cm^2 corneal ED_{50} was 0.19, 0.42, 1.18, 2.31, and 3.82 s, respectively.

Model results for short and long time intervals are shown for 1318 and 1150 nm CW laser radiation for various powers delivered to the cornea in Figs. 9–11. Param-

eters were for 1318 and 1150 nm CW laser radiation, in Figs. 9 and 11 and in Fig. 10, respectively, into a human eye with a $1/e^2$ Gaussian beam radius of 2.12 mm at the virtual cornea. Unless specifically stated in the caption, all parameters in the remaining model results were the same, save for the absorption coefficients and index of refraction due to dispersion. In Fig. 11, all parameters were identical to those used to produce the model results in Fig. 9, except the value of dn/dT was doubled from -4.46×10^{-5} to -8.92×10^{-5} K^{-1}.
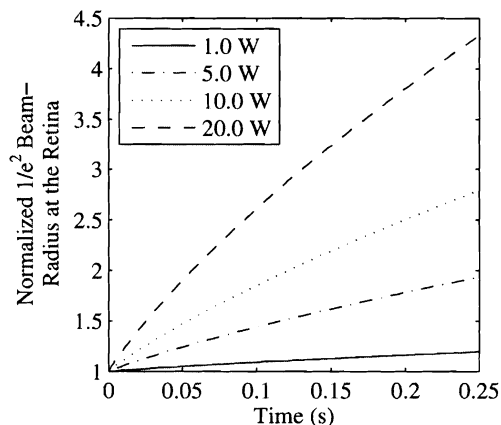

Fig. 7.   Increase in the beam radius at the retina as a function of time for selected powers delivered to the cornea. Parameters were for 1318 nm CW laser radiation into a human eye, with a $1/e^2$ Gaussian beam radius of 2.12 mm at the virtual cornea. The y axis was normalized to 98 μm, which was the beam radius at the virtual retina determined at time zero.
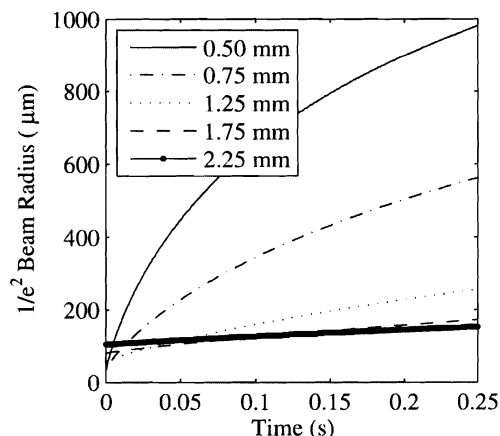

Fig. 8.   Increase in the beam radius at the retina as a function of time for selected input beam radii at the cornea.
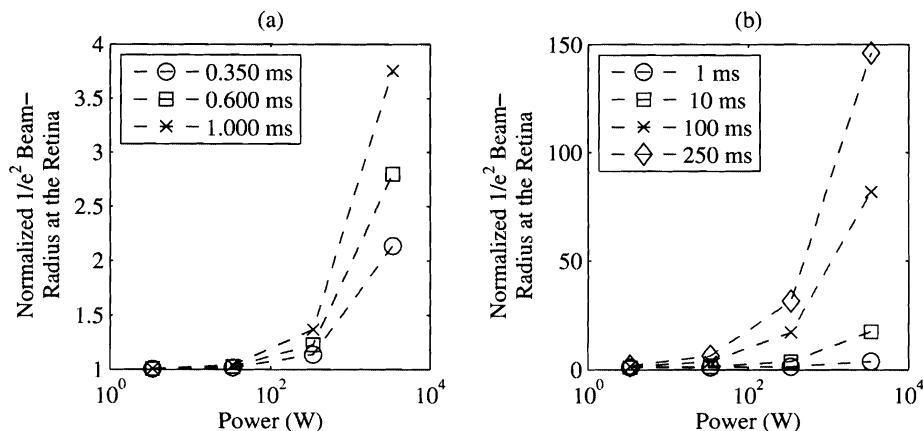
Fig. 9.   Increase in the beam radius for 1318 nm laser radiation at the retina as a function of input power at the cornea for (a) short time ($t \leqslant 1$ ms) and (b) long time (1 ms$<t\leqslant$250 ms). Note the 340 W power at 0.350 ms approximates the ED_{50} threshold level reported in Zuclich *et al.* [34] for the equivalent wavelength. The y axis was normalized to the initial beam radius of 98 μm.
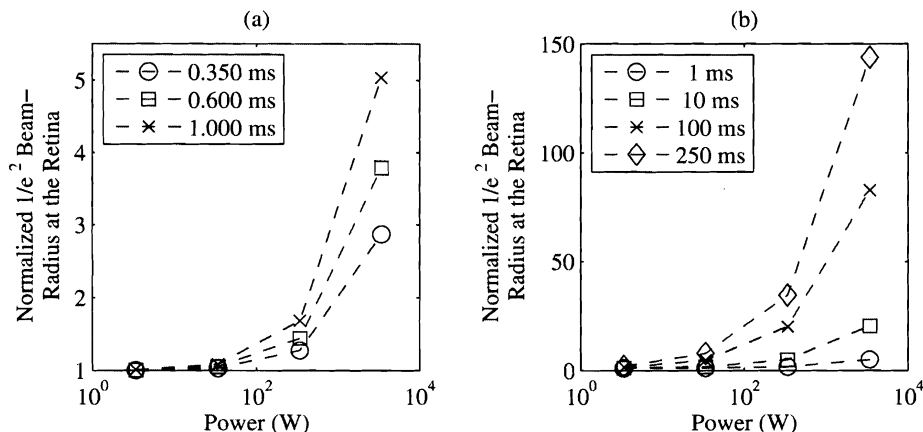

Fig. 10.   Increase in the beam radius for 1150 nm laser radiation at the retina as a function of input power at the cornea for (a) short time ($t \leqslant 1$ ms) and (b) long time (1 ms$<t\leqslant$250 ms). The y axis was normalized to the initial beam radius of 82 μm.
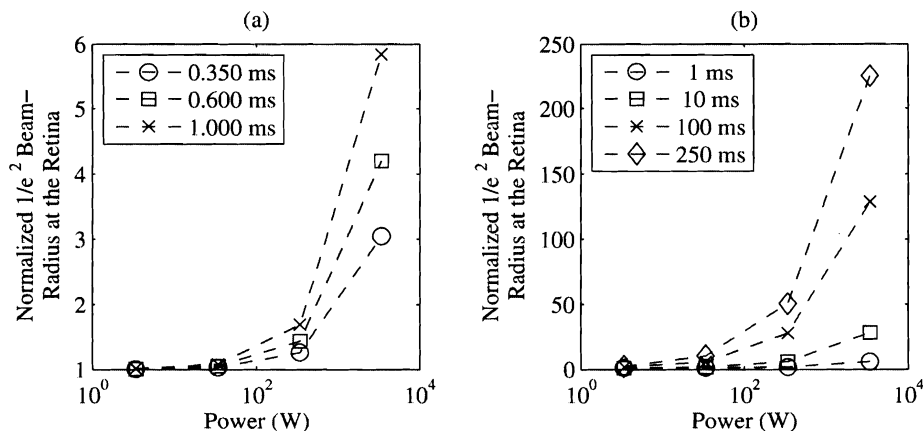

Fig. 11.   Increase in the beam radius for 1318 nm laser radiation at the retina as a function of input power at the cornea for (a) short time ($t \leqslant 1$ ms) and (b) long time (1 ms$<t\leqslant$250 ms) having doubled the value of dn/dT to -8.92×10^{-5} K^{-1}. The y axis was normalized to the initial beam radius of 98 μm.

5. DISCUSSION

Analysis of the Schiebener *et al.* data for $n(T,\lambda,P)$ revealed three trends for water in the liquid phase between 283 and 363 K at pressures from 0.1 to 0.2 MPa (see Fig. 4 for dn/dT at 0.1 MPa). First, the modulus of the thermo-optic coefficient $|dn/dT|$ decreases with increasing wavelength for laser radiation between 400 and 2325 nm. Second, the modulus of the thermo-optic coefficient increases as temperature increases for liquid water and finally, decreases very slightly as pressure increases from 0.1 to 0.2 MPa. This suggests the magnitude of dn/dT for ocular media at body temperature and standard ocular pressures should be approximately two times greater than dn/dT values for water held in a cuvette at room temperature (see vertical lines in Fig. 4). Understanding these fundamental trends will lend insight into predicting thermal lensing trends in the eye.

Using data from Schiebener *et al.* as a guide, an estimate for dn/dT at a wavelength of 1313 nm between 290–293 K (room temperatures) and pressures near 1 atm ($\sim$0.1 MPa) was found to be between -6.96×10^{-5} and -7.86×10^{-5} K^{-1} (see Fig. 4). The dn/dT value of -4.46×10^{-5} K^{-1} determined to yield the best fit to z-scan data (used for modeling results in Figs. 5 and 6) comes close to this range of dn/dT values. The error associated with the selected value for dn/dT is very difficult to quantify given the sensitivity of the z-scan data to the optical alignment of the system. Misalignment in the optical system for the z-scan would introduce aberrations not accounted for in the first-order model, which considers only a Gaussian wavefront. Further, it has been demonstrated that thermal lensing in water results in convective flow processes introducing nonlinear aberrations into the steady-state reading [20,35–37].

Though the standard deviation of the normalized intensity for the experimental z-scan measurements was ±0.02 arbitrary units, there are limitations of the closed-aperture z-scan. Measures were taken to minimize errors including routine optical alignment checks before every data collection and careful knife-edge measurements to characterize the laser beam profile. However meticulous these measures were, they cannot account for the uncertainty with the beam's deflection due to convectional effects projected onto a stationary aperture. Convection causes small deflections in the beam's alignment along the x and y directions, giving rise to a nonlinear asymmetric temperature profile, that are magnified over the long distance to the aperture in the far field. For conditions involving higher input power and longer exposure times, such as the 48 mW case in Figs. 5 and 6, the thermal lens causes the profile of the beam to break its Gaussian distribution, forming a donut shape [20,35–37]. The closed-aperture z-scan cannot account for or detect conditions where the Gaussian wavefront is compromised. Alfonso *et al.* reported using a thin vertical slit in place of the iris aperture shown in Fig. 2 to overcome this problem; however, slit length was constrained by the physical dimensions of the detector [37]. Given these limitations of the single-beam-closed-aperture z-scan, our future thermal lensing investigations will utilize a variation on the z-scan to observe a nonlinear beam profile. Current alter-native investigational methods are being evaluated and will be reported at a later date.

The strength in the formation of the nonlinear beam profile has been shown to be directly related to the exposure length, power of the radiation source, and absorptivity of the exposed media [20,35–37]. For this reason, z-scan data were collected for low (2.6 mW) and high (48 mW) power. The condition of a symmetric beam profile is more likely to be maintained in the low-power data set. Comparing the low- to high-power z-scan data [Figs. 5(a) and 5(b), respectively], it is evident the amount of overestimation by the model in the low-power case is much less than in the high-power case. The model in the low-power transient result [Fig. 6(a)] overestimated the z-scan irradiance data by less than 1% compared with the more than 18% overestimated by the model in the high-power data set at 1 s [Fig. 6(c)]. The low-power z-scan data appear noisier than the high-power data because the irradiance levels were dipping toward the lower limit of the detector. When the limitations of the single-beam, closed-aperture z-scan are considered, the results from the first-order, thermal-lensing, z-scan model suggests our model provides a good estimate for the strength of the thermal lens effect. The dn/dT value of -4.46×10^{-5} K^{-1} found in the fit is a reasonable estimate for trends in thermal lensing effects in the eye. With the consideration of imperfections in the optical system and the formation of asymmetric beam profiles, it is prudent to discuss the uncertainty associated with our model's results.

Our first-order model's limitations include the fact that we assume radial symmetry is maintained throughout the exposure, neglect heat conduction along the z axis, and treat the eye as a simple system of homogenous slabs with a single curved surface placed on the cornea. The creation of the asymmetric temperature and nonlinear beam profiles mean our mathematical solution based on radially symmetric profiles becomes invalid. The use of the simple eye model affords a straightforward propagation of the beam profile, reducing the complexity of an already difficult heat conduction problem in the creation of the thermal lens. The first-order thermal lensing results from the simple eye assist us in approximating the magnitude of the effect the thermal lens may have on the size of the laser beam radius at the retina in an eye exposed to CW NIR laser radiation. It should be stressed that the eye is a more complex optical system than the simple model presented here. Advanced models of the eye can be found in Artal *et al.*, Tabernero *et al.*, and, for a case detailing chromatic correction in the near infrared, in Fernández *et al.* [38–40].

More advanced models of thermal lensing in ocular media to include heat conduction along the z-axis and the nonlinear beam profile are currently underway. As the fidelity of the thermal lensing model is increased, the complexity and computational needs, including resources and time, of the model are increased. The first-order model is computationally inexpensive and fits our z-scan data reasonably well, particularly for the low-power z-scan experimental data in Figs. 5(a) and 6(a). Regardless of the first-order model's limitations, we find it suitable for assessing trends of thermal lensing in the eye caused by near-infrared laser radiation.

From model results shown in Fig. 7, it is evident the magnitude of thermal lensing increases with power. For strongly absorbed wavelengths, the fluence at the retina can vary significantly with input power and time of the exposure. The power levels presented in Fig. 7 were chosen to represent the range of power—up to the limit of the CW 1318 nm laser source—used in the retinal damage studies conducted by Zuclich *et al.* [3,34]. Note at 20 W under the simulated conditions, the beam's $1/e^2$ radius doubles from 98 μm to 196 μm at approximately 56 ms and is more than four times larger than initial state after 250 ms. Retinal damage threshold studies were never successful on primates for CW 1318 nm, and it has never been understood what the mechanisms were that limited damage [1]. Model results from Fig. 7 suggest that the fluence rate delivered to the retina would decrease over time, potentially preventing damage to the retina.

The input beam diameter significantly influences the thermal lensing effect as illustrated in Fig. 8. The trend is revealed as a constant-power Gaussian input beam decreases in radius at the cornea: the magnitude of the thermal lens greatly increases as a result of the increased heat source along the optical axis. This is not surprising given the physics of the z-scan. The most dramatic impact of the thermal lens occurs inside the focus and is even described as the reason for creating z-scan systems in which the sample is shorter than the depth of focus of the system [12]. Thus, as the depth of focus (DOF) increases, the magnitude of the thermal lens inside the media should increase as well. The DOF is given as $2\pi\lambda(f_\lambda/2d)^2$, where f_λ is the focal length of the virtual eye for the respective wavelength λ, and d is the input diameter of the laser beam at the virtual cornea. Initially, at time zero, the smaller input radii delivered to the cornea produce the smallest laser spot at the virtual retina. At some point in time, the conditions with the longer DOF at the virtual retina will give the larger thermal lens. This suggests that when calculations are made to increase the fluence delivered to the retina for strongly-absorbed laser radiation, the condition of decreasing the input laser beam radius may in fact be decreasing the delivered fluence due to the thermal lens.

Zuclich *et al.* reported for a 1315 nm wavelength with a 350 μs retinal exposure, the ED$_{50}$ is 0.844 J/cm^2 delivered at the retina [3]. Taking this value and scaling it to the $1/e^2$ beam radius of 2.1 mm indicates that 0.119 J was delivered to the cornea. Dividing by an exposure time of 350 μs provides an average power of 340 W. A series of powers input at the cornea for four different magnitudes, including this 340 W case, are shown in Fig. 9. It takes only 3 ms before the beam radius at the virtual retina doubles in size. As power increases, the thermal lens will develop faster. Zuclich *et al.* were able to determine retinal damage thresholds for short-pulsed (<1 ms), 1318 nm laser radiation since the time for the thermal lens to manifest itself is significantly longer than the pulse duration of the laser source.

In Figs. 9 and 10, the model was run for four different orders of magnitude in input power at the cornea for 1318 and 1150 nm laser radiation wavelengths, respectively, to demonstrate how the change in absorption and depth of focus affects the thermal lens. The absorption coefficients

for the components of the eye in Fig. 3 for 1150 and 1318 nm laser radiation are given in Table 2. Less than 2% of the 1318 nm radiation reaches the virtual retina compared with the near 7% energy transmitted at 1150 nm [1]. Given the trends in literature from Schiebener *et al.* for dn/dT, the value of dn/dT should be slightly greater for 1150 nm compared with 1318 nm. Even with the value of dn/dT being the same for both wavelengths, these results can provide information on the behavior of the thermal lens. Figures 9 and 10 show that the 1150 nm radiation begins to invoke the thermal lens more strongly for times less than 250 ms, but at the 250 ms point, the magnitude of the thermal lens is very close to the model results of the 1318 nm radiation case. Overall, the results in Fig. 9 and 10 suggest there is no large variation in the degree of thermal lensing between 1318 and 1150 nm laser radiation.

Analysis of Fig. 4 suggests that the value of the dn/dT modulus doubles from room to body temperatures. The simulations run for Figs. 9 and 11 were identical save for the fact that dn/dT was -4.46×10^{-5} and -8.92×10^{-5} K^{-1}, respectively. Doubling the magnitude of dn/dT caused the $1/e^2$ beam-waist radius results in Fig. 11(b) to be approximately 33% larger at 250 ms than the comparable results in Fig. 9(b). These results demonstrate that, all things being equal, the magnitude of the thermal lens does increase, but is not proportional to the modulus of the thermo-optic coefficient.

6. CONCLUSION

Our mathematical model was found to fit experimental z-scan data reasonably well for a dn/dT value of -4.46×10^{-5} (K^{-1}) for water at room temperature exposed to 1313 nm CW laser radiation. This value is close to the predicted dn/dT values based on analysis of the Schiebener *et al.* data (Fig. 4) [16]. The trends from Fig. 4 suggest the value of dn/dT for water at body temperature is approximately two times greater than the dn/dT value for water at room temperature. This conservative value of dn/dT, -4.46×10^{-5} K^{-1} lends information on trends of thermal lensing in the human eye exposed to CW laser radiation in the 1150–1350 nm region. Our model provides a reasonable first-order approximation of the trends of the thermal lensing effect on the fluence rate delivered to the retina. The thermal lens causes the fluence rate delivered to the retina to decrease over time, potentially preventing damage to the retina for NIR exposures when sufficient time is allowed for thermal lensing to occur. Modeling results show the thermal lens takes several ms to develop. Retinal damage studies conducted by Zuclich *et al.* on nonhuman primates were successful for exposure durations less than a ms, but could never explain a retinal lesion for exposures greater than 100 ms [34]. Based on our results, the CW 1318 nm laser radiation retinal damage studies for exposures greater than 100 ms may have been affected by a decreasing delivered retinal fluence rate precluding damage.

REFERENCES

1. R. L. Vincelette, B. A. Rockwell, R. J. Thomas, D. J. Lund, and A. J. Welch, "Thermal lensing in ocular media exposed to continuous-wave near-infrared radiation: 1150–1350 nm region," J. Biomed. Opt. **13**, 054005 (2008).

2. C. D. Clark, L. J. Irvin, P. D. S. Maseberg, G. D. Buffington, R. J. Thomas, M. L. Edwards, and J. Stolarski, "BTEC Thermal Model," Report AFRL-RH-BR-TR-2008-0006 (Air Force Research Laboratory, San Antonio, 2008).

3. J. A. Zuclich, D. J. Lund, and B. E. Stuck, "Wavelength dependence of ocular damage thresholds in the near-IR to far-IR transition region: Proposed revisions to MPEs," Health Phys. **92**, 15–23 (2007).

4. D. J. Lund, P. Edsall, and B. E. Stuck, "Spectral dependence of retinal thermal injury," Proc. SPIE **3902**, 22–34 (2000).

5. D. J. Lund and P. Edsall, "Action spectrum for retinal thermal injury," Proc. SPIE **3591**, 324–334 (1999).

6. J. P. Gordon, R. C. Leite, R. S. Moore, S. P. Porto, and J. R. Whinnery, "Long transient effects of lasers with inserted liquid samples," J. Appl. Phys. **36**, 3–8 (1965).

7. D. Kovsh, S. Yang, D. J. Hagan, and E. W. Van Stryland, "Nonlinear optical beam propagation for optical limiting," Appl. Opt. **38**, 5168–5180 (1999).

8. D. I. Kovsh, D. J. Hagan, and E. W. Van Stryland, "Numerical modeling of thermal refraction in liquids in the transient regime," Opt. Express **4**, 315–327 (1999).

9. H. L. Fang and R. Swofford, "Analysis of the thermal lensing effect for an optically thick sample-A revised model," J. Appl. Phys. **50**, 6609–6615 (1979).

10. W. D St. John, B. Taheri, J. P. Wicksted, R. C. Powell, D. H. Blackburn, and D. C. Cranmer, "Time-dependent thermal lensing in lead oxide-modified silicate glass," J. Opt. Soc. Am. B **9**, 610–616 (1992).

11. A. Yariv, *Quantum Electronics*, 3rd ed. (Wiley, 1989), pp. 106–123.

12. M. Franko and C. D. Tran, "Analytical thermal lens instrumentation," Rev. Sci. Instrum. **67**, 1–18 (1996).

13. G. M. Hale and M. R. Querry, "Optical constants of water in the 200-nm to 200-μm wavelength region," Appl. Opt. **12**, 555–563 (1973).

14. A. H. Harvey, J. S. Gallagher, and J. M. H. Levelt Sengers, "Revised formulation for the refractive index of water and steam as a function of wavelength, temperature and density," J. Phys. Chem. Ref. Data **27**, 761–774 (1998).

15. W. Wagner and A. Kruse, *Properties of Water and Steam: The Industrial Standard IAPWS-IF97 for the Thermodynamic Properties and Supplementary Equations for Other Properties* (Springer-Verlag, 1998), p. 150.

16. P. Schiebener, J. Straub, J. M. H. Levelt Sengers, and J. S. Gallagher, "Refractive index of water and steam as function of wavelength, temperature and density," J. Phys. Chem. Ref. Data **19**, 677–717 (1990).

17. E. F. Maher, "Transmission and absorption coefficients for the ocular media of the Rhesus monkey," Tech. Rep. SAM-TR-78-32 (USAF School of Aerospace Medicine, 1978).

18. R. L. Vincelette, R. J. Thomas, B. A. Rockwell, and A. J. Welch, "A comparison of a first-order thermal lensing model to a closed aperture Z-scan for the propagation of light in ocular media," Proc. SPIE **6084**, 0G1–0G9 (2006).

19. R. J. Thomas, R. L. Vincelette, G. D. Buffington, A. D. Strunk, M. A. Edwards, B. A. Rockwell, and A. J. Welch, "A first order model of thermal lensing of laser propagation in the eye and implications for laser safety," in *International Laser Safety Conference* (Laser Institute of America, 2005), 147–154.

20. R. L. Vincelette, R. J. Thomas, B. A. Rockwell, and A. J. Welch, "Thermal lensing in the ocular media," Proc. SPIE **6435**, 0C1–7 (2007).

21. R. J. Thomas, R. L. Vincelette, C. D. Clark, III, J. Stolarski, L. J. Irvin, and G. D. Buffington, "Propagation effects in the assessment of laser damage thresholds to the eye and skin," Proc. SPIE **6435**, A1–12 (2007).

22. W. C. Lin, "Dynamics of tissue optics during laser heating," Ph.D. dissertation (University of Texas, Austin, Texas, 1997).

23. M. A. Porras, J. Alda, and E. Bernabeu, "Nonlinear propagation of arbitrary laser beams by means of the generalized *ABCD* formalism," Appl. Opt. **32**, 5885–5892 (1993).

24. P. A. Belanger, "Beam propagation and the *ABCD* ray matrices," Opt. Lett. **16**, 196–198 (1991).

25. H. A. Wyld, *Mathematical Methods for Physics* (W. A. Benjamin, 1976), pp. 319–326.

26. J. V. Beck, K. D. Cole, A. Haji-Sheikh, and B. Litkouhi, *Heat Conduction Using Green's Functions* (Hemisphere Publishing Corp., 1992), pp. 201–216.

27. R. L. Swofford and J. Morrell, "Analysis of the repetitively pulsed dual-beam thermo-optical absorption spectrometer," J. Appl. Phys. **49**, 3667–3674 (1978).

28. M. Sheik-Bahae, A. A. Said, T.-H. Wei, D. J. Hagan, and E. W. Van Stryland, "Sensitive measurement of optical nonlinearities using a single beam," IEEE J. Quantum Electron. **26**, 760–769 (1990).

29. D. A. Atchison and G. Smith, *Optics of the Human Eye* (Elsevier, 2002).

30. G. Li, H. Zwick, B. Stuck, and D. J. Lund, "On the use of schematic eye models to estimate retinal image quality," J. Biomed. Opt. **5**, 307–314 (2000).

31. G. Westheimer, "The Eye: Including Central Nervous System Control of Eye Movements," in *Medical Physiology*, Vol. 1, V. B. Mountcastle, ed., 14th ed. (C. V. Mosby Company, 1980), pp. 482–503.

32. E. J. Fernández, A. Unterhuber, P. M. Prieto, B. Hermann, W. Drexler, and P. Artal, "Ocular aberrations as a function of wavelength in the near infrared measured with a femtosecond laser," Opt. Express **13**, 400–409 (2005).

33. T. Okuno, M. Kojima, I. Hata, and D. H. Sliney, "Temperature rises in the crystalline lens from focal irradiation," Health Phys. **88**, 214–222 (2005).

34. J. A. Zuclich, D. J. Lund, B. E. Stuck, and P. R. Edsall, "Ocular effects and safety standard implications for high-power lasers in the 1.3–1.4 μm wavelength range," (Air Force Research Laboratory, Laser Radiation Branch, San Antonio, Texas, 2004).

35. M. Motamedi, A. J. Welch, W. F. Cheong, S. A. Ghaffari, and O. T. Tan, "Thermal lensing in biological medium," IEEE J. Quantum Electron. **24**, 693–696 (1988).

36. C. E. Buffett and M. D. Morris, "Convective effects in thermal lens spectroscopy," Appl. Spectrosc. **37**, 455–458 (1983).

37. E. F. S. Alfonso, M. A. R. Revert, M. C. G. Alvarez-Coque, and G. R. Ramos, "Reduction of convective low-frequency noise in thermal lens spectrometry," Appl. Spectrosc. **44**, 1501–1507 (1990).

38. P. Artal, A. Benito, and J. Tabernero, "The human eye is an example of robust optical design," J. Vision **6**, 1–7 (2006).

39. J. Tabernero, P. Piers, A. Benito, M. Redondo, and P. Artal, "Predicting the optical performance of eyes implanted with IOLS to correct spherical aberration," Invest. Ophthalmol. Visual Sci. **47**, 4651–4658 (2006).

40. E. J. Fernandez, A. Unterhuber, B. Povazay, B. Hermann, P. Artal, and W. Drexler, "Chromatic aberration correction of the human eye for retinal imaging in the near infrared," Opt. Express **14**, 6213–6225 (2006).